Magnetic Resonance in Medicine 51:559–567 (2004)

Parallel Imaging Reconstruction Using Automatic Regularization

Fa-Hsuan Lin,[1–3*] Kenneth K. Kwong,[2,3] John W. Belliveau,[2,3] and Lawrence L. Wald[2,3]

Increased spatiotemporal resolution in MRI can be achieved by the use of parallel acquisition strategies, which simultaneously sample reduced *k*-space data using the information from multiple receivers to reconstruct full-FOV images. The price for the increased spatiotemporal resolution in parallel MRI is the degradation of the signal-to-noise ratio (SNR) in the final reconstructed images. Part of the SNR reduction results when the spatially correlated nature of the information from the multiple receivers destabilizes the matrix inversion used in the reconstruction of the full-FOV image. In this work, a reconstruction algorithm based on Tikhonov regularization is presented that reduces the SNR loss due to geometric correlations in the spatial information from the array coil elements. Reference scans are utilized as a priori information about the final reconstructed image to provide regularized estimates for the reconstruction using the L-curve technique. This automatic regularization method reduces the average *g*-factors in phantom images from a two-channel array from 1.47 to 0.80 in twofold sensitivity encoding (SENSE) acceleration. In vivo anatomical images from an eight-channel system show an averaged *g*-factor reduction of 1.22 to 0.84 in 2.67-fold acceleration. Magn Reson Med 51:559–567, 2004. © 2004 Wiley-Liss, Inc.

Key words: SENSE; regularization; *g*-factor; parallel MRI; L-curve

The use of multiple receivers in MRI can be exploited to enhance spatiotemporal resolution by reducing the number of *k*-space acquisitions. The folded image that would result from conventional reconstruction is avoided by the use of spatial information from multiple coils. Several methods for using this information have been proposed, including the *k*-space-based simultaneous acquisition of spatial harmonics (SMASH) method (1,2) and the image domain-based sensitivity encoding (SENSE) approach (3). By reducing sampling time, these parallel MRI techniques can be used to reduce image distortion in echo-planar imaging (EPI) (4) or diminish acoustic noise by lowering gradient switching rates (5). However, these advantages come at the cost of a reduced signal-to-noise ratio (SNR). The reduction in SNR stems from two factors: the reduced number of data samples, and the instability in reconstruction due to correlations in the spatial information as determined by the geometrical arrangement of the array coil. The first is the inevitable result of reducing the number of samples. The second might be affected by optimizing coil geometry (6,7) or improving the stability of the reconstruction algorithm. The increased noise originating from correlated spatial information from the array elements can be estimated based on knowledge of the array geometry, and is quantified by the geometric factor (*g*-factor) map (3).

The reconstruction of parallel MRI can be formulated as linear equations (8) that must be inverted to obtain an unfolded image from the reduced *k*-space data set. If the matrix is well conditioned, the inversion can be achieved with minimal amplification of noise. While the encoding matrix can still be inverted even if it is nearly singular, in this ill-conditioned case, small noise perturbations in the measured data (aliased image) can produce large variations in the full-FOV reconstruction. This effect causes noise amplifications in regions of the image where the encoding matrix is ill-conditioned.

The restoration of full-FOV images requires the use of additional information, such as the coil sensitivity maps provided by a low-spatial-resolution, full-FOV reference scan. In addition to being required to determine the coil sensitivity profile that becomes part of the linear equations to be inverted, the reference scan may also provide a priori information that is useful for regularizing the inversion process. In this work, we present a framework for mitigating the noise amplification in SENSE reconstruction by utilizing Tikhonov regularization (9). The advantage of regularized parallel MRI reconstructions was previously reported in a study on cardiac imaging in which an empirical formula of a fixed fraction (0.05) of the first eigenvalue was used (2). Similarly, regularized SENSE reconstruction using an empirical regularization parameter was described by King (10). The benefits of incorporating prior information to reduce the noise level of reconstructed images have also been demonstrated (10–12). Furthermore, it has been reported that regularization can potentially be used to unfold aliased images from an underdetermined system (i.e., the aliased pixel number exceeds the RF channels in the array) (13). Nevertheless, no systematic approach has been described to provide a regularization parameter for SENSE image reconstruction, and spatial distribution of noise arising from unfolding SENSE images has not been well characterized when regularization is employed. In this study, we employed a full-FOV reference scan and the L-curve algorithm (14) to determine the optimum regularization parameter. In addition, we demonstrated the effect of regularization on the noise of the unfolded images by *g*-factor maps using both phantom and in vivo experimental data.

[1]Division of Health Sciences and Technology, Harvard Medical School-MIT, Cambridge, Massachusetts.

[2]Department of Radiology, Massachusetts General Hospital, Charlestown, Massachusetts.

[3]Athinoula A. Martinos Center for Biomedical Imaging, Massachusetts General Hospital, Harvard Medical School-MIT, Charlestown, Massachusetts.

Grant sponsor: National Center for Research Resources; Grant number: P41RR14075; Grant sponsor: Mental Illness and Neuroscience Discovery (MIND) Institute.

*Correspondence to: Fa-Hsuan Lin, Athinoula A. Martinos Center for Biomedical Imaging, Bldg. 149 13th Street, Mailcode 149-2301, Charlestown, MA 02129. E-mail: fhlin@mit.edu

Received 21 March 2003; revised 13 October 2003; accepted 13 October 2003.

DOI 10.1002/mrm.10718
Published online in Wiley InterScience (www.interscience.wiley.com).

THEORY

The formation of aliased images from multiple receivers in parallel MRI can be formulated as a linear operation to "fold" the full-FOV spin density images (8).

$$\vec{y} = A\vec{x} \qquad [1]$$

Here $\vec{y}$ is the vector formed from the pixel intensities recorded by each receiver (folded image), and $\vec{x}$ is the vector formed from the full-FOV image. The encoding matrix A consists of the product of the aliasing operation due to subsampling of the k-space data and coil-specific sensitivity modulation over the image. The goal of the image reconstruction is to solve for $\vec{x}$ given our knowledge of A, which is derived from understanding the folding process and an estimate of the coil sensitivity maps. While Eq. [1] is expressed in the image domain SENSE approach (3), similar linear relationships are formed in the k-space-based SMASH (1,2) method. Furthermore, the same basic formalism is used in either the in vivo sensitivity method (2), or conventional SENSE/SMASH methods requiring coil sensitivity estimation. In general, Eq. [1] is an overdetermined linear system, i.e., the number of array coils, which is the row dimension of $\vec{y}$, exceeds the number of the pixels that fold into the measured pixel, the row dimension of $\vec{x}$.

To solve for $\vec{x}$ (the full-FOV image), the overdetermined matrix is inverted using a least-squares estimation (3):

$$\begin{aligned}\vec{x} &= U\vec{y} \\ &= (A^H\Psi^{-1}A)^{-1}A^H\Psi^{-1}\vec{y},\end{aligned} \qquad [2]$$

where the superscript H denotes the transposed complex conjugate, and Ψ is the receiver noise covariance (3). When Ψ is positive semi-definite, the eigen decomposition of the receiver noise covariance leads to the unfolding matrix, U, using the whitened aliasing operator $\tilde{A}$ and the whitened observation $\tilde{y}$.

$$\begin{aligned}\Psi &= V\Lambda V^H \\ \tilde{A} &\equiv \Lambda^{-1/2}V^HA \\ \tilde{y} &\equiv \Lambda^{-1/2}V^H\vec{y} \\ \vec{x} &= U\tilde{y} \\ &= (\tilde{A}^H\tilde{A})^{-1}\tilde{A}^H\tilde{y}.\end{aligned} \qquad [3]$$

The whitening of the aliasing operator will be used in the regularization formulation introduced in the next section. The whitening incorporates the receiver noise covariance matrix, implicitly allowing optimal SNR reconstruction within the regularization formulation. The noise sensitivity of the parallel imaging reconstruction is thus quantified by the amplification of the noise power due to the geometry of the array. This g-factor is thus written as (3)

$$g_{\rho\rho} = \frac{\sqrt{X^{parallel\ imaging}_{\rho\rho}}}{\sqrt{R}\sqrt{X^{full}_{\rho\rho}}} = \sqrt{[(\tilde{A}^H\tilde{A})^{-1}]_{\rho\rho}(\tilde{A}^H\tilde{A})_{\rho\rho}}\,. \qquad [4]$$

The subscript ρ indicates the voxels to be "unfolded" in the full-FOV image, and $\boldsymbol{X}$ denotes the covariance of the reconstruction image vector $\vec{x}$. Here R denotes the factor by which the number of samples is reduced (the acceleration rate).

Tikhonov Regularization

Tikhonov regularization (9) provides a framework for stabilizing the solution of ill-conditioned linear equations. The solution of Eq. [1] using Tikhonov regularization can be written as

$$\vec{x}^{\lambda} = \underset{\vec{x}}{\operatorname{argmin}}\ \{\|\tilde{A}\vec{x} - \vec{\tilde{y}}\|_2 + \lambda^2\|L(\vec{x} - \vec{x}^0)\|_2\}. \qquad [5]$$

Here λ^2 is the regularization parameter, L is a positive semi-definite linear transformation, $\vec{x}^0$ denotes the prior information about the solution $\vec{x}$, and $\|\bullet\|_2$ represents the L-2 norm. Thus the second term in Eq. [5], defined as the prior error, is the deviation of the solution image from the prior knowledge. The first term, defined as the model error, represents the deviation of the observed aliased image from the model observation. The model observation is a folded version of the solution image. The regularization parameter determines the relative weights with which these two estimates of error combine to form a cost function.

Consider the extreme case when λ^2 is zero and we attempt to minimize only the first term. This is equivalent to solving the original equation, $\vec{y} = A\vec{x}$, without conditioning (conventional SENSE reconstruction). At the other extreme, when λ^2 is large, the solution will be a copy of the prior information $\vec{x}^0$. Thus, the regularization parameter λ^2 quantifies the trade-off between the error from prior knowledge not describing the current image, and the error from noise amplification from the unconditioned matrix inversion. An appropriate choice of λ^2 (regularization) decreases the otherwise complete dependency on the whitened model ($\tilde{A}$) and the whitened observation ($\tilde{y}$) to constrain the solution to within a reasonable "distance" from the prior knowledge ($\vec{x}^0$). Thus the regularization increases the influence of prior-knowledge, full-FOV image information during the unfolding of the aliased images.

Given the regularization parameter λ^2, and letting L be an identity matrix, the solution of Eq. [4] is written as (14)

$$\begin{aligned}\vec{x}^{\lambda} &= \sum_{j=1}^{n}\left(f_j\frac{\vec{u}_j^H\tilde{y}}{s_{jj}} + (1-f_j)\vec{v}_j^H\vec{x}^0\right)\vec{v}_j \\ f_j &= \frac{s_{jj}^2}{s_{jj}^2+\lambda^2} \cong \begin{cases} 1, & S_{jj}\gg\lambda \\ s_{jj}^2/\lambda^2, & S_{jj}\ll\lambda \end{cases}.\end{aligned} \qquad [6]$$

Here $\vec{u}_j$, $\vec{v}_j$, and s_{jj} are the left singular vectors, right singular vectors, and singular values of $\tilde{A}$, respectively, generated by singular value decomposition (SVD), with singular values and singular vectors indexed by j. This leads to the ollowing matrix presentations:

$$\begin{aligned}\vec{x}^{\lambda} &= V\Gamma U^H\tilde{y} + V\Phi V^H\vec{x}^0 \\ VAR(\vec{x}^{\lambda}) &= V\Gamma^2V^H \\ \Gamma_{ii} &= \frac{f_i}{s_{ii}} = \frac{s_{ii}}{s_{ii}^2+\lambda^2}\,. \\ \Phi_{ii} &= 1 - f_i = \frac{\lambda^2}{s_{ii}^2+\lambda^2}\end{aligned} \qquad [7]$$

Using regularization and Eq. [4], the ratio of the noise levels between the regularized parallel MRI reconstruction and the original full-FOV image normalized by the factor of acceleration gives the local geometry factor for noise amplification:

$$g_{\rho\rho} = \sqrt{[(V\Gamma^2V^H)]_{\rho\rho}[(VS^2V^H)]_{\rho\rho}}. \quad [8]$$

Inside the square root of Eq. [8], the first square bracket term denotes the variance of the unfolding using regularization from Eq. [7], and the second square bracket term denotes the variance of the full-FOV reference image.

Estimating the Optimal Regularization Parameter Using the L-Curve

To determine the appropriate regularization parameter λ^2, we utilized the L-curve approach (14). Qualitatively, we expect that as regularization increases, more dependency on the prior information leads to a smaller discrepancy between the prior information and the solution, at the cost of a larger difference between model prediction and observation. Similarly, a small regularization parameter decreases the difference between model prediction and observation at the cost of a larger discrepancy between the prior information and the solution. The L-2 norm is used to quantify the difference between these vectors. The model error and prior error can then be calculated (14) using:

$$\rho \equiv \|\tilde{y} - \tilde{A}\vec{x}\|_2 = \sum_{j=1}^{n} ((1 - f_j)u_j^H\tilde{y})^2$$

$$\eta \equiv \|\vec{x} - \vec{x}^0\|_2 = \sum_{j=1}^{n} \left(f_j\left(\frac{u_j^H\tilde{y}}{s_{jj}} - \vec{x}_j^0\right)\right)^2, \quad [9]$$

where $\vec{x}_j^0$ is the jth element of prior $\vec{x}^0$.

Plotting model error vs. prior error for a range of λ^2 shows the available trade-offs between the two types of error. A representation of this plot, termed the L-curve, is shown in Fig. 1. The optimal regularization parameter is defined as that which strives to minimize and balance the two error terms. This occurs at the elbow of the L-curve. Mathematically, this is where its curvature is minimal. The analytic formula (14) for the L-curve's curvature enables a computationally efficient search to be performed for the λ^2 at the point of minimal curvature.

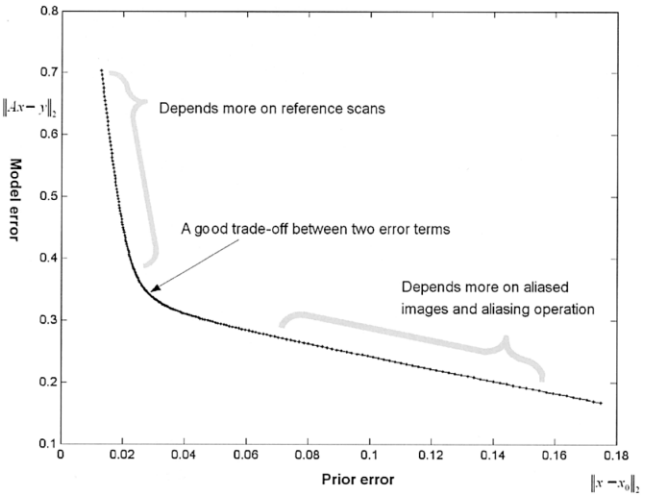

FIG. 1. An L-curve illustrates the two costs during reconstruction of the aliased images from an array. Using distinct regularization, the reconstruction biases toward minimizing either the prior error or the model error. A trade-off between these two error metrics is the use of regularization at the "corner" of the L-curve.

MATERIALS AND METHODS

Phantom studies were performed on a 1.5T clinical MRI scanner (Siemens Medical Solutions, South Iselin, NJ) using an in-house-made, two-element array. Each element was a circular surface coil (5.5-cm diameter) tuned to the Larmor frequency of the scanner. The two element coils had a 1.5-cm overlap to minimize inductive coupling. The array was mounted on curved plastic with a curvature radius of 20 cm to conform the phantom and subjects. A 2D gradient-echo sequence was used to image the homogenous, spherical (11.6-cm diameter) saline phantom. The imaging parameters were TR = 100 ms, TE = 10 ms, flip angle = 10°, slice thickness = 3 mm, FOV = 120 mm × 120 mm, and image matrix = 256 × 256. The same scan was repeated with the number of phase-encode lines reduced to 75%, 62.5%, and 50%.

The in vivo anatomical images were acquired using a 3T scanner (Siemens Medical Solutions) with an eight-channel linear phased-array coil wrapped around the whole brain circumferentially. Each circular surface coil element was 9 cm in diameter and tuned to the proton Larmor frequency at 3T. Appropriate overlapping between neighboring coils minimized mutual inductance between coil elements. We used a fast low-angle shot (FLASH) 3D sequence to acquire in vivo brain images from a healthy subject, after approval from the Institutional Review Board and informed consent from the subject were obtained. The parameters of the FLASH sequence were TR = 500 ms, TE = 3.9 ms, flip angle = 20°, slice thickness = 3 mm with a 1.5-mm gap, 48 slices, FOV = 210 mm × 210 mm, and image matrix = 256 × 256. The same scan was repeated with the number of phase-encode lines reduced to 50%, 37.5%, and 25%.

We adopted in vivo sensitivity reconstructions for both the phantom and in vivo experiments to avoid potential increases in the *g*-factor due to misestimation of the coil sensitivity maps (2). Also, to illustrate the validity of utilizing prior information while avoiding the complications of different spatial resolutions, we employed identical spatial resolutions for both reference scans and accelerated acquisitions. While the use of a full-resolution reference scan defeats the purpose of the SENSE acceleration for standard radiographic imaging, it is useful for time-series imaging applications, such as fMRI. However, to demonstrate the effect of regularization when only a low-resolution full-FOV reference scan is available, we also apply the regularization method to a reconstruction using lower-resolution full-FOV reference images. For this demonstra-

tion, we downsampled the full-FOV reference images by two- or fourfold (from a 256 × 256 matrix to 128 × 128 and 64 × 64 matrices) and employed the lower-resolution reference images as priors in 2.00- and 2.67-fold accelerated acquisitions.

The use of regularization allows a smooth trade-off between replication of the reference information and noise introduced in the poorly-conditioned inversion that may result from reliance on the measured data alone. Therefore, it is important to have some indication that there is not an overreliance on the reference data (i.e., that the regularization parameter is not extremely high). For the fMRI application, the time-series data should not simply replicate the reference data, in which case subtle temporal changes in the time-series would not be detected (functional CNR would be lowered).

To test the degree to which regularization might reduce the CNR in an fMRI study, we simulated a 2.00-fold-accelerated SENSE fMRI scan consisting of 50 time points for the baseline (resting) and active conditions. An image from the eight-channel array was used as a template to construct the 100-image time series. Model activation was added to half of the images by increasing the pixel value by 10% in a 4-pixel region of interest (ROI) in the occipital lobe of the left hemisphere. White Gaussian noise of zero mean was added to the time-series, and the images were reconstructed with and without the regularization method. A two-sample *t*-test between the active and baseline conditions was used to measure fMRI sensitivity.

In practice, we calculate the L-curve by iteratively calculating the two terms in the cost function (Eq. [9]) after performing SVD on the whitened encoding matrix. The search range of the regularization parameter was restricted to a range between the largest and smallest singular values. The search was done in a 200-sample geometric sequence, each term of which is given by a multiple of the previous one. The curvature associated with each sample was computed. Subsequently, the minimal curvature was found within this search range. Image reconstruction, matrix regularization, and computation of the *g*-factor maps were performed on a Pentium-III $1GH_Z$ dual processor Linux system with code written in MATLAB (Mathworks, Natick, MA).

RESULTS

Figure 2 shows the reconstructed full-FOV phantom images and the associated *g*-factor maps from the 1.5T scanner using the spherical saline phantom and two-element surface coil array employing 1.33-fold (192 lines), 1.60-fold (160 lines), and 2.00-fold (128 lines) accelerations. Although the overall image SNR in this acquisition was relatively high near the surface coils, SENSE reconstruction noise arising from matrix inversion was significantly improved by the regularization step for all of the accelerated acquisitions (1.33-fold, 1.60-fold, and 2.00-fold accelerations). The effect of the regularization step was greatest for the SENSE reconstruction at 2.00-fold acceleration. The largest reductions in noise were observed near the coil. The bottom panel of Fig. 2 shows the *g*-factor maps for regularized and nonregularized reconstructions. The *g*-factor maps are all scaled by the same factor to facilitate comparison. The regularized reconstructions allow *g*-factors of <1, since prior knowledge is used. In contrast, the conventional nonregularized reconstructions always have a minimum *g*-factor of 1. Table 1 summarizes the *g*-factor average, standard deviation, and median in 1.33-fold, 1.60-fold, and 2.00-fold accelerations. For the 1.33-fold acceleration case, the regularization provided an average 87% reduction in the added reconstruction noise. For the 2.00-fold acceleration case, the regularization provided an average 1.84-fold reduction.

Figure 3 shows the regularized and nonregularized reconstructed in vivo images and *g*-factor maps from the 3T scanner using the eight-channel array coil with 2.67- and 2.00-fold accelerations. The *g*-factor maps showed noticeable local decreases in the added noise levels of the regularized reconstructed images. Similarly, regularization helped reduce noise in the temporal lobe in 2.67-fold acceleration (middle panel). In 4.00-fold acceleration, regularized reconstruction demonstrated decreased noise in the deep temporal lobe inside the insular cortex. Table 2 summarizes the *g*-factor average, standard deviation, and median in the reconstructed anatomical images. As expected, more accelerated acquisitions resulted in higher *g*-factors in both regularized and nonregularized reconstructions. In 2.00-fold acceleration, the *g*-factor average was suppressed from 1.07 to 0.72 by regularization (49% reduction). In 4.00-fold acceleration, the *g*-factor-associated noise reduction by regularization was 31% (nonregularized: 2.04, regularized: 1.52). Here, the SNR advantages resulting from regularized reconstruction can be appreciated in the temporal lobe of the anatomical images (Fig. 4). In 2.00-fold acceleration, a banded noise region in the nonregularized reconstruction was minimized (Figs. 3 and 4). The calculated L-curve is shown in Fig. 1 for a representative set of aliased pixels for the 2.0-fold accelerated case.

The SENSE reconstructions using lower-spatial-resolution reference scans are shown in Fig. 5 and Table 3. In 2.00-fold acceleration using a reference scan at 50% of the spatial resolution of the accelerated acquisition, the average *g*-factor was reduced by the regularization method from 1.08 to 0.73. When the reference scan with 25% of the spatial resolution of the 2.00-fold accelerated acquisition was employed, the average *g*-factor was reduced from 1.10 to 0.73. For the higher acceleration (2.67-fold) case, a reference scan of 50% of the spatial resolution resulted in an average *g*-factor of 1.21. Regularization reduced this to 0.86.

In this simple fMRI model data, the contrast reduction resulting from replication of the reference image was compensated for by the lower noise in the regularized reconstruction. A two-sample *t*-test between the active and baseline conditions showed that the use of regularization increased the *t*-statistics from 5.93 to 6.77.

For a full-FOV image with a matrix size of 256 × 256, the computation times for estimating the regularization parameters were 72 min, 45 min, and 26 min for the 2.00-, 2.67-, and 4.00-fold accelerations, respectively. After the regularization parameters were estimated, it took 44, 34, and 24 min to reconstruct a single-slice, single-measurement aliased image at 2.00-, 2.67-, and 4.00-fold accelerations, respectively, including calculations of both regular-

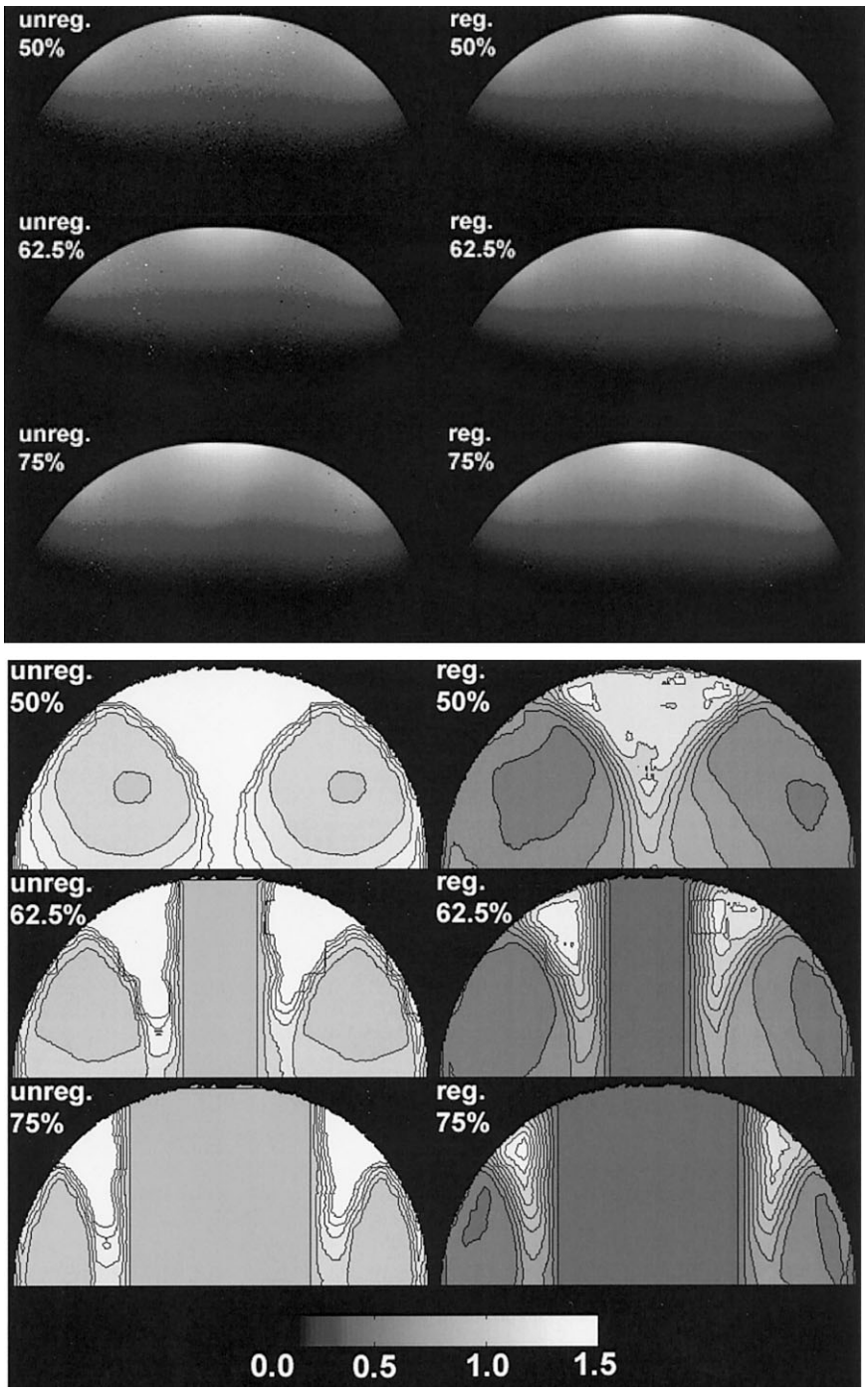

FIG. 2. The reconstructed phantom images and *g*-factor maps using unregularized or regularized reconstruction in 50%, 62.5%, and 75% phase encoding.

ized and nonregularized unfolded images and their associated *g*-factor maps.

DISCUSSION

The regularization approach introduced in this work was intended to minimize SNR loss by constraining the matrix inversion. Mathematically, this is equivalent to obtaining a compromise between an expected a priori result and the noisy result from inversion with no conditioning. Such an approach is equivalent to the maximal a posteriori (MAP) estimation in stochastic Bayesian modeling. The "optimal" solution in this scenario thus implies the simultaneous minimization of model errors and prior errors, which is graphically represented at the elbow of the L-curve. The proposed regularized parallel MRI reconstruction algorithm is expected to be universally workable, and independent of the *k*-space sampling scheme, the array coil configuration, and the imaging anatomy. In the regularized SENSE reconstruction, we found that *g*-factors can be smaller than 1. A *g*-factor of 1 indicates that the reconstruction added no additional noise due to the operation of unfolding the aliased image alone. A *g*-factor of <1, which can occur when regularization is employed, indicates that

Table 1
G-factors in Unregularized and Regularized SENSE Reconstructions From Phantom Images Using a 2-channel Phased Array Coil at 50%, 62.5%, and 75% Phase Encoding

Acceleration	Unregularized			Regularized		
	Mean	SD	Median	Mean	SD	Median
2.00	1.47	1.56	1.17	0.80	0.52	0.67
1.60	1.43	1.96	1.07	0.76	0.65	0.60
1.33	1.31	1.27	1.00	0.70	0.58	0.50

Table 2
G-factors in Unregularized and Regularized SENSE Reconstructions From In Vivo Images Using an 8-channel Phased Array Coil at 25%, 37.5%, and 50% Phase Encoding

Acceleration	Unregularized			Regularized		
	Mean	SD	Median	Mean	SD	Median
2.00	1.07	0.12	1.02	0.72	0.25	0.66
2.67	1.22	0.23	1.14	0.84	0.31	0.98
4.00	2.04	0.58	1.94	1.52	0.53	1.52

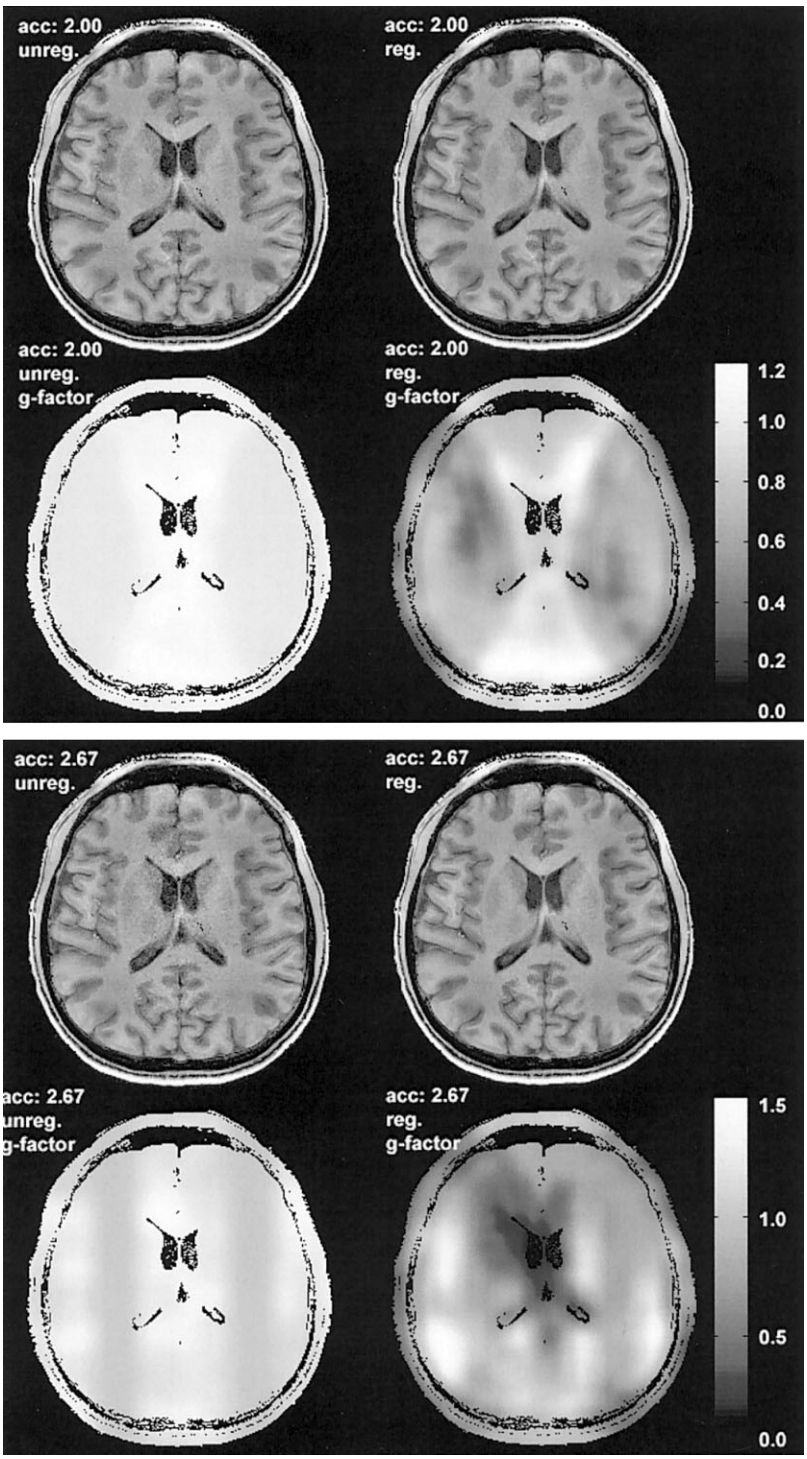

FIG. 3. The reconstructed in vivo images and *g*-factor maps using unregularized or regularized reconstruction in 37.5% (top panel) and 50% (bottom panel) phase encoding.

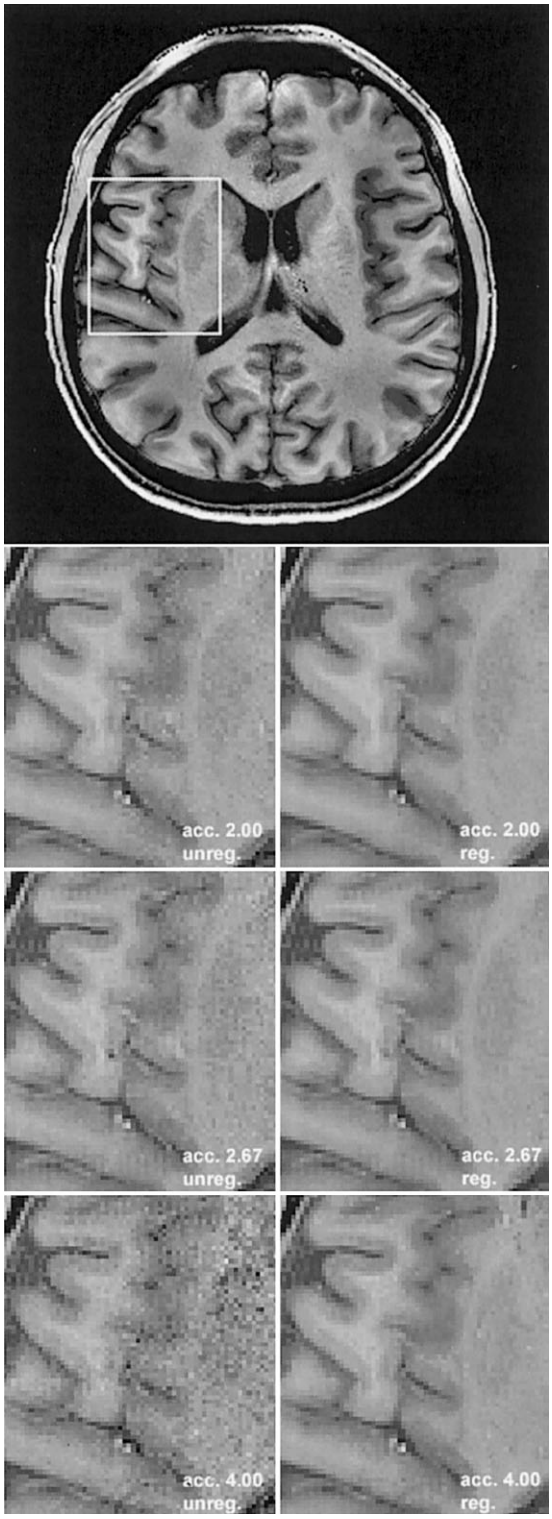

FIG. 4. The selected temporal lobe area from the whole brain image as shown by the white box (top panel). Detailed anatomy from unregularized and regularized SENSE reconstructions of 2.00-, 2.67-, and 4.00-fold accelerations.

the unfolding operation itself decreases the stochastic variability of the estimated spin density compared to the full-FOV reference scans. This reduction in noise results from the prior knowledge used in the regularization process. From the original definition of the *g*-factor, when excluding the effect of number of samples (or the acceleration factor, *R*) in the denominator of the first term in Eq. [4], the *g*-factor is the ratio of the variance of the estimated spin density from parallel acquisitions over the variance of the spin density from the full-FOV reference scan. Since prior information is employed in the regularized parallel MRI reconstruction, less variability of the estimated spin density from parallel acquisitions is expected. Thus, the use of regularization can partially compensate for the SNR loss due to the reduced samples in the accelerated acquisition. It is important to note that this reduction reflects the use of prior knowledge, which may lead to a biased result. A potential concern with the use of regularization is that image features of the reference scan may be replicated in the reconstructed image. This bias is seen as imparted image blurring in Fig. 5 for the high-acceleration-rate reconstruction using four-fold lower-spatial-resolution reference images. For an fMRI time-series experiment, later time-points might be biased toward the first reference image, reducing the contrast between the activated and resting state. The model fMRI data set analyzed here suggests, however, that the CNR of the time series is improved by the regularization procedure. Thus the contrast reduction is less important than the noise reduction due to regularization. Another concern with the use of regularization in parallel MRI reconstruction is that the noise in the prior reference itself could at some point be introduced into the reconstruction, thereby limiting the visible SNR improvements. However, the quality of the full-FOV prior image can be improved either by multiple averages if parallel MRI is used for dynamic imaging applications, or by spatial smoothing using kernels with dimensions similar to the signal, based on the matched-filter theory.

The advantage of using regularized parallel MRI reconstructions was previously reported by Sodickson (2) in a study on cardiac imaging, in which an empirical formula of a fraction (0.05) of the first eigenvalue was used. Similarly, regularized SENSE reconstruction using an empirical regularization parameter was described by King (10). Subsequently, other studies have demonstrated the benefits of prior information in parallel MRI reconstructions (11–13,15). In contrast to fixed regularization strategies, we have utilized an automatic regularization implemented by mathematically and computationally convenient algorithms to stabilize the image reconstruction. This is expected to be more adaptable to different anatomy and coil configurations.

In this study, we utilized the so-called "in vivo SENSE" reconstruction approach described by Sodickson (2). This method substitutes a priori information for the detailed estimate of the coil profile used by SENSE (3). In the uniform phantom, the two methods are identical, since the full-FOV a priori image is identical to a coil profile map. We chose the in vivo sensitivity reconstruction approach to demonstrate the with/without regularization in unfolding effects in "in vivo SENSE" because 1) the *g*-factor gains are independent of problems incurred from misestimation of the coil sensitivity profiles; 2) the inclusion of the phantom study demonstrates regularization in both "traditional" SENSE and in vivo SENSE, since in vivo SENSE reduces to a form of traditional SENSE in this case; and 3)

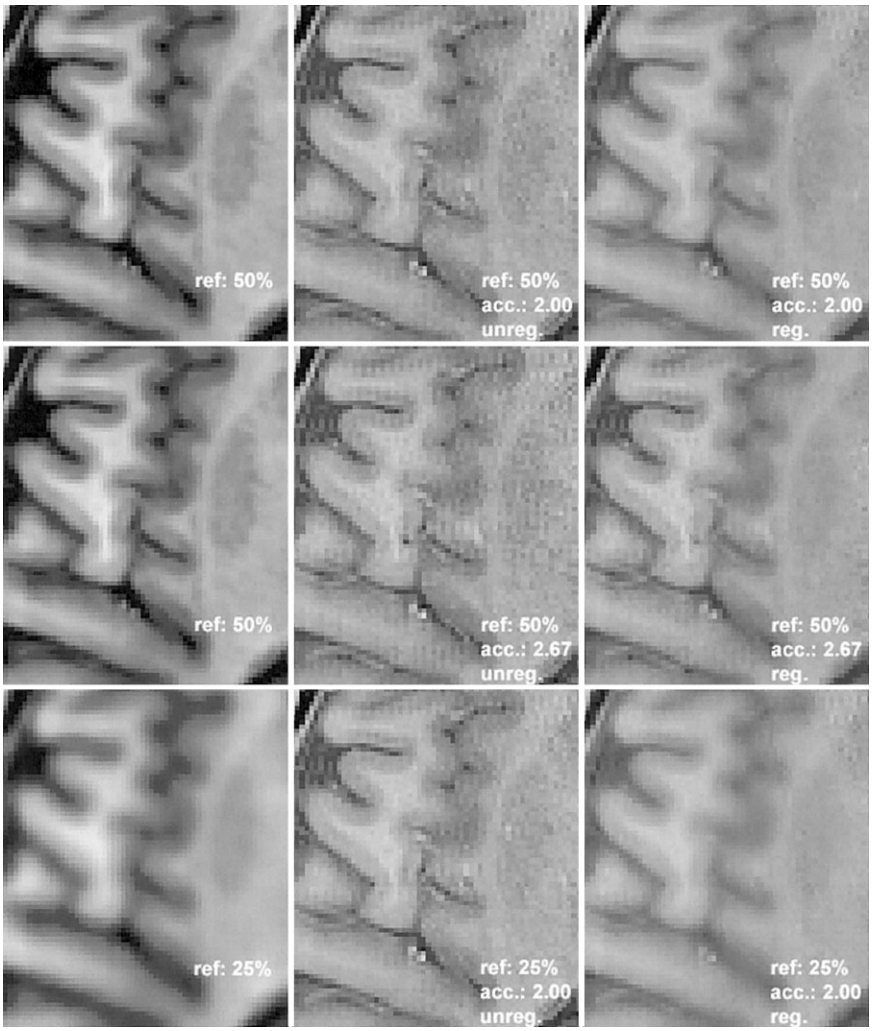

FIG. 5. Detailed temporal lobe anatomy from unregularized and regularized SENSE reconstructions of 2.00- and 2.67-fold accelerations using reference scans at 50% and 25% spatial resolution of the accelerated acquisitions.

the in vivo SENSE method has an intrinsic appeal for time-series measurements (such as fMRI), where only small intensity changes are expected relative to the baseline image.

In the current experiments, our regularization approach worked robustly with different field strengths and array coil configurations, and the benefits of reduced *g*-factor-associated SNR loss were consistently observed. Once the regularization parameters are determined, the computational reconstruction time is identical to the reconstruction without regularization. Thus the additional computational demand for the proposed technique is the total time needed to estimate the regularization parameters. The long computational time required for even unregularized inversion using MATLAB shows that this environment is useful only for testing the method. Note that our unfolding of aliased SENSE images includes a calculation of both regularized and nonregularized reconstructions and their associated *g*-factor maps. The computation time can be reduced to 1/4 of the reported time if only one set of the unfolded full-FOV image is estimated. Computational speed may be further improved by optimizing code platform. Even given the closed-form model errors and prior errors in Eq. [9], searching through different λ^2's is neces-

Table 3
G-factors in Unregularized and Regularized SENSE Reconstructions From In Vivo Images Using an 8-channel Phased Array Coil at 2-fold and 2.67-fold Acceleration Using Reference Image of Lower Spatial Resolutions

Acceleration	Reference image resolution	Unregularized			Regularized		
		Mean	SD	Median	Mean	SD	Median
2.00	100%	1.07	0.12	1.02	0.72	0.25	0.66
2.00	50%	1.08	0.15	1.02	0.73	0.26	0.66
2.00	25%	1.10	0.20	1.01	0.73	0.27	0.67
2.67	100%	1.22	0.23	1.14	0.84	0.31	0.98
2.67	50%	1.21	0.23	1.14	0.86	0.31	1.01

sary to locate the minimal curvature. This could be made more efficient by the use of a direct regularization estimation method. In dynamic imaging, the impact on the increased image reconstruction time due to regularization estimation can be minimized by estimating regularizations only once, and then using identical regularization parameters for the repeated time points. This is particularly attractive for functional brain activation studies, in which the changes with time are quite small. In addition to the proposed L-curve technique, other automatic regularization estimation methods, such as generalized cross validation (GCV) (16,17), can potentially be used to obtain appropriate regularization estimations.

CONCLUSIONS

In this work we present an approach to employ regularization in reconstructing parallel MRI data in order to reduce the noise amplification of the reconstruction (*g*-factor). The proposed L-curve algorithm was fully automatic and showed a significant reduction in average *g*-factors in phantom and in vivo data at 1.5T and 3T. For some pixels the *g*-factor was reduced to <1, indicating that the a priori knowledge in the reconstruction reduced the variability below that of the full-FOV reference scan. The reliance on a priori knowledge did not, however, reduce functional imaging CNR in a model fMRI experiment. Although the method was demonstrated using the in vivo SENSE method, the regularization method for reducing noise amplification may be beneficial for most variants of parallel MR reconstruction. The use of the lower spatial full-FOV reference image as the regularization prior information at large accelerations may result in oversmoothed reconstructed images, leading to a loss of spatial resolution.

ACKNOWLEDGMENTS

F.-H. Lin thanks Michael A. Ohliger of the Beth Israel Deaconess Medical Center for helpful discussions.

REFERENCES

1. Sodickson DK, Manning WJ. Simultaneous acquisition of spatial harmonics (SMASH): fast imaging with radiofrequency coil arrays. Magn Reson Med 1997;38:591–603.
2. Sodickson DK. Tailored SMASH image reconstructions for robust in vivo parallel MR imaging. Magn Reson Med 2000;44:243–251.
3. Pruessmann KP, Weiger M, Scheidegger MB, Boesiger P. SENSE: sensitivity encoding for fast MRI. Magn Reson Med 1999;42:952–962.
4. Kellman P, McVeigh ER. Ghost artifact cancellation using phased array processing. Magn Reson Med 2001;46:335–343.
5. de Zwart JA, van Gelderen P, Kellman P, Duyn JH. Reduction of gradient acoustic noise in MRI using SENSE-EPI. Neuroimage 2002;16:1151–1155.
6. Weiger M, Pruessmann KP, Leussler C, Roschmann P, Boesiger P. Specific coil design for SENSE: a six-element cardiac array. Magn Reson Med 2001;45:495–504.
7. de Zwart JA, Ledden PJ, Kellman P, van Gelderen P, Duyn JH. Design of a SENSE-optimized high-sensitivity MRI receive coil for brain imaging. Magn Reson Med 2002;47:1218–1227.
8. Sodickson DK, McKenzie CA. A generalized approach to parallel magnetic resonance imaging Med Phys 2001;28:1629–1643.
9. Tikhonov AN, Arsenin VI. Solutions of ill-posed problems. Washington/New York; Winston, distributed by Halsted Press. 1977.
10. King K. SENSE image quality improvement using matrix regularization. In: Proceedings of the 9th Annual Meeting of ISMRM, Glasgow, Scotland, 2001. p 1771.
11. Tsao J, Pruessmann K, Boesiger P. Prior-information-enhanced dynamic imaging using single or multiple coils with k-t BLAST and k-t SENSE. In: Proceedings of the 10th Annual Meeting of ISMRM, Honolulu, 2002. p 2369.
12. Lin F-H, Kwong KK, Chen Y-J, Belliveau JW, Wald LL. Reconstruction of sensitivity encoded images using regularization and discrete time wavelet transform estimates of the coil maps. In: Proceedings of the 10th Annual Meeting of ISMRM, Honolulu, 2002. p 2389.
13. Katscher U, Manke D. Underdetermined SENSE using a-priori knowledge. In: Proceedings of the 10th Annual Meeting of ISMRM, Honolulu, 2002. p 2396.
14. Hansen PC. Rank-deficient and discrete ill-posed problems: numerical aspects of linear inversion. Philadelphia; SIAM. 1998.
15. Liang Z-P, Bammer R, Ji J, Pelc N, Glover G. Making better SENSE: wavelet de-noising, Tikhonov regularization, and total-least squares. In: Proceedings of the 10th Annual Meeting of ISMRM, Honolulu, 2002. p 2388.
16. Golub GH, Heath MT, Wahba G. Generalized cross-validation as a method for choosing a good ridge parameter. Technometrics 1979;21:215–223.
17. Wahba G. Practical approximate solutions to linear operator equations when the data are noisy. SIAM J Numer Anal 1977;14:651–667.